

# *Long-term culture of pluripotent stem-cell-derived human neurons on diamond – a substrate for neurodegeneration research and therapy*

Article

Published Version

Creative Commons: Attribution 4.0 (CC-BY)

Open Access

Nistor, P. A., May, P. W., Tamagnini, F., Randall, A. D. and Caldwell, M. A. (2015) Long-term culture of pluripotent stem-cell-derived human neurons on diamond – a substrate for neurodegeneration research and therapy. *Biomaterial*, 61. pp. 139-149. ISSN 0142-9612 doi: <https://doi.org/10.1016/j.biomaterials.2015.04.050> Available at <http://centaur.reading.ac.uk/80570/>

It is advisable to refer to the publisher's version if you intend to cite from the work.

To link to this article DOI: <http://dx.doi.org/10.1016/j.biomaterials.2015.04.050>

Publisher: Elsevier

All outputs in CentAUR are protected by Intellectual Property Rights law, including copyright law. Copyright and IPR is retained by the creators or other copyright holders. Terms and conditions for use of this material are defined in the [End User Agreement](#).

[www.reading.ac.uk/centaur](http://www.reading.ac.uk/centaur)

**CentAUR**

Central Archive at the University of Reading

Reading's research outputs online



# Long-term culture of pluripotent stem-cell-derived human neurons on diamond – A substrate for neurodegeneration research and therapy



Paul A. Nistor<sup>a, b</sup>, Paul W. May<sup>b, \*</sup>, Francesco Tamagnini<sup>c</sup>, Andrew D. Randall<sup>c, d</sup>,  
Maev A. Caldwell<sup>a, e, \*\*</sup>

<sup>a</sup> Regenerative Medicine Laboratory, School of Clinical Sciences, University of Bristol, Bristol BS8 1TD, United Kingdom

<sup>b</sup> School of Chemistry, University of Bristol, Bristol BS8 1TS, United Kingdom

<sup>c</sup> The Hatherly Labs, School of Medical Sciences, University of Exeter, Exeter EX4 4EA, United Kingdom

<sup>d</sup> Department of Physiology and Pharmacology, University of Bristol, Bristol BS8 1TD, United Kingdom

<sup>e</sup> Trinity College Institute of Neuroscience, Lloyd Institute, Trinity College, Dublin 2, Ireland

## ARTICLE INFO

### Article history:

Received 6 February 2015

Received in revised form

24 April 2015

Accepted 30 April 2015

Available online 20 May 2015

### Keywords:

Pluripotent stem cells

Diamond substrate

Boron-doped diamond

Neuronal differentiation

Long term culture

Neuronal survival

Neurodegeneration research

## ABSTRACT

Brain Computer Interfaces (BCI) currently represent a field of intense research aimed both at understanding neural circuit physiology and at providing functional therapy for traumatic or degenerative neurological conditions. Due to its chemical inertness, biocompatibility and stability, diamond is currently being actively investigated as a potential substrate material for culturing cells and for use as the electrically active component of a neural sensor. Here we provide a protocol for the differentiation of mature, electrically active neurons on microcrystalline synthetic thin-film diamond substrates starting from undifferentiated pluripotent stem cells. Furthermore, we investigate the optimal characteristics of the diamond microstructure for long-term neuronal sustainability. We also analyze the effect of boron as a dopant for such a culture. We found that the diamond crystalline structure has a significant influence on the neuronal culture unlike the boron doping. Specifically, small diamond microcrystals promote higher neurite density formation. We find that boron incorporated into the diamond does not influence the neurite density and has no deleterious effect on cell survival.

© 2015 The Authors. Published by Elsevier Ltd. This is an open access article under the CC BY license (<http://creativecommons.org/licenses/by/4.0/>).

## 1. Introduction

In the past 10 years diamond has emerged as a biomaterial targeted towards neural implants [1–3], driven by the maturing technology of chemical vapour deposition (CVD) which allows thin films of diamond to be deposited relatively inexpensively over areas of many square cm [4,5]. Inherent to diamond are a number of characteristics which make it a desirable substrate for tissue implantation. Diamond is not chemically reactive, it is not immunogenic and it is stable over extremely long periods of time. This means that a diamond prosthesis will very likely survive the patient [6–10]. Considering diamond's extreme rigidity, such prostheses

would be unsuitable for implantation into moving parts of the body and, would be best suited for Brain Computer Interfaces (BCI). An attractive feature of diamond is that while it is electrically insulating in its pure form, it can be made conductive by doping with atoms that could act either as donors or acceptors of electrons and thus, able to conduct electrical impulses from/to adjacent cells [11,12]. The advantage of this method is that the conductive and insulating part of an electrode would be made of the same bioinert material. Rodent and human neurons, derived from neural progenitors and neural stem cells, have been successfully cultured on diamond or diamond like carbon substrates [1,2,13–17], and have been reported to grow along pre-patterned diamond or diamond like carbon stripes to form 2D neural networks [18]. Recently, a boron-doped diamond probe implanted in rodents in contact with the cerebral cortex for six months has been shown to be free of any major histological or physiological side-effects [3], and a diamond retinal prosthesis has been proposed [19]. Furthermore, nitrogen included ultrananocrystalline diamond and boron doped diamond

\* Corresponding author.

\*\* Corresponding author. Regenerative Medicine Laboratory, School of Clinical Sciences, University of Bristol, Bristol BS8 1TD, United Kingdom.

E-mail addresses: [paul.may@bristol.ac.uk](mailto:paul.may@bristol.ac.uk) (P.W. May), [maeve.caldwell@bristol.ac.uk](mailto:maeve.caldwell@bristol.ac.uk) (M.A. Caldwell).

have been shown to induce less fibrotic encapsulation than silicon [20].

Of note, diamond's unusual properties make it a potentially much more useful substrate than a simple replacement for the current titanium cortical implants. Specifically two “*in vitro*” lines of investigation are currently open. One involves the study of the direct interaction of neurons with the substrate, both mechanically and electrically, towards optimization of the probes of the future. The other involves the study of neuronal aging and degeneration in an electro-physiological context on a diamond multi-electrode array (MEA). Both these lines of investigation are dependent on the long-term culture of specific types of mature human neurons. However, the extreme sensitivity to “*in vitro*” manipulation and very limited availability of human mature neurons, as well as the limited differentiation potential of neural progenitors, are significant constraining factors. Therefore, the ideal solution would be the “*in vitro*” generation of mature neurons from pluripotent stem cells.

Currently there are two sources of human pluripotent cells: epiblast-derived human embryonic stem cells (hESC) and adult cells converted “back to pluripotency”, also termed human induced-pluripotent stem cells (hiPS). hiPS are pluripotent cells derived from adult donors which allow both “*in vitro*”, highly reproducible studies of specific diseases, as well as transplantation back into the patient, free of host-versus-graft reaction.

Since neuronal differentiation from pluripotent cells reflects the long human development, any differentiation protocol would have to face the challenges of extended time in culture; *i.e.* over 100 days. Currently, human pluripotent cells are being differentiated into various neuronal subtypes in monolayer, on plastic and in defined chemical conditions. Following the successful culture of mammalian neural cells on diamond substrates [1,2,13–15,17,18] it could be inferred that differentiation towards neuronal fates from human pluripotent cells should also be possible on these substrates. However, the optimal conditions that would support human neurons in long-term culture are currently unknown.

Furthermore, cell response to diamond doped with boron, an electron acceptor, is also poorly understood. Boron is an element with dose-dependent toxicity. In laboratory animals, boron compounds have been found to be toxic only at very high doses [21,22], while in humans, studies of workers chronically exposed to relatively high levels, failed to demonstrate pathological consequences [23,24]. However, exposure to boron leads to accumulation in the brain [25] and, *in vitro* testing indicated that boron nanotubes are more toxic than carbon nanotubes to cells in culture [26].

We present here a protocol for differentiation of human IPS cells into cortical neurons on microcrystalline diamond and investigate the role of diamond structure in this process. We also show that diamond doped with boron, an electron acceptor, does not adversely influence either the differentiation process or the health and viability of the neurons.

## 2. Material and methods

### 2.1. Diamond characterization

Commercial diamond was purchased from Element Six, Ltd., either as a single-crystal plate (P2, 145-500-0055), or as a polycrystalline smooth-polished diamond plate (TM-CVD 145-500-0090). These were compared with the in-house produced diamond as previously described [4]. Briefly, a thin diamond film was deposited on a silicon wafer (Silicon Materials <100>) in a hot filament reactor using standard chemical vapour deposition (CVD) conditions (1%CH<sub>4</sub> in H<sub>2</sub>, 2.67 kPa pressure, filament temperature 2400 K, substrate temperature ~1100 K, for 2–12 h). This produced an insulating, continuous microcrystalline diamond film at a rate of

about 0.5 μm h<sup>-1</sup>. For boron-doped diamond 2000 ppm diborane gas was added to the mixture which increased the conductivity of the diamond film to near-metallic [27].

All samples were then cleaned in concentrated nitric acid (68% v/v). The as-grown hydrogen-terminated diamond surface was then converted to a predominantly oxygen-terminated surface, as previously described [2], by exposing the sample to ozone for 20 min (UVO cleaner, Jetlight Co. 42A-220). Previous reports [2] have shown that oxygen-terminated diamond surfaces are preferable for cell survival.

To test the best diamond structure for neural culture we made use of a feature of diamond CVD that the size of the crystals produced depends on the deposition time. To that effect, we employed a hot filament reactor to grow polycrystalline diamond films for times ranging between 2 and 12 h (Fig. 1, and Suppl. Fig. 1). The supportive properties of the in-house diamond were compared with those of a polycrystalline smooth-polished diamond (Suppl. Fig. 2).

The diamond crystals were imaged by scanning electron microscopy (SEM), using a Quanta 400FEI system. To quantitatively assess the size of the crystals produced, two complementary methods were used: measurement of the average distance between the sharp peaks of 2 adjacent crystals, and counting the number of sharp peaks within an area of 1 μm<sup>2</sup> (Fig. 2). We speculated that these are the parameters with most biological significance, as the sharp corners of the crystal facets are the most conspicuous structural features a cell will encounter. The boron-doped diamond crystals (Suppl. Fig. 1) were slightly larger than the corresponding undoped crystals grown for the same amount of time. However, quantification indicated that although larger, the boron-doped diamond crystals were not large enough to match the size of the next tier of undoped diamond crystals (Suppl. Fig. 3).

### 2.2. Raman spectroscopy

The Raman spectra were measured at room temperature by means of a Renishaw spectrometer. The samples were excited using an argon-ion laser at λ = 515.5 nm. The laser power was set to 6 mW and the spot size to 15 μm. The spectra for undoped and B-doped diamond (Fig. 3) are consistent with high quality microcrystalline diamond films with little or no graphitic impurities [28].

### 2.3. ES/IPS cell culture

We set out to adapt the current protocols for differentiating human pluripotent cells towards neuronal lineages [29–31] to the specifics of a diamond substrate. Furthermore, a requirement for cells used for regenerative medicine is that they are cultured in fully defined conditions free of animal components (xeno-free). Human pluripotent cells are routinely cultured on a feeder layer of mouse embryonic fibroblasts (MEFs) in Knock-Out Serum Replacement (KOSR), which contains bovine serum albumin (BSA). Consequently, the culture conditions are neither defined nor xeno-free. A feeder-free system has been applied successfully (TeSR) [32]. However, this system uses Matrigel as a substrate (a poorly defined matrix of animal origin) and requires BSA. Recently, two fully defined, xeno-free systems became commercially available: Essential 8™ (LifeTechnologies) [33] and, StemFit™ (Ajinomoto Co., Inc.) [34]. However, most protocols for neuronal differentiation from hiPS use KOSR-based media as the starting point.

Three pluripotent lines have been used for this study: ES-Shef6 (MRC Stem Cell Bank), IPS-MSU (Michigan State University) and IPS-NAS2 (Dr. Tilo Kunath laboratory) [35]. Cells were maintained in xeno-free and feeder-free E8 medium as recommended by the manufacturer (LifeTechnologies, A1517001). Briefly, cells were

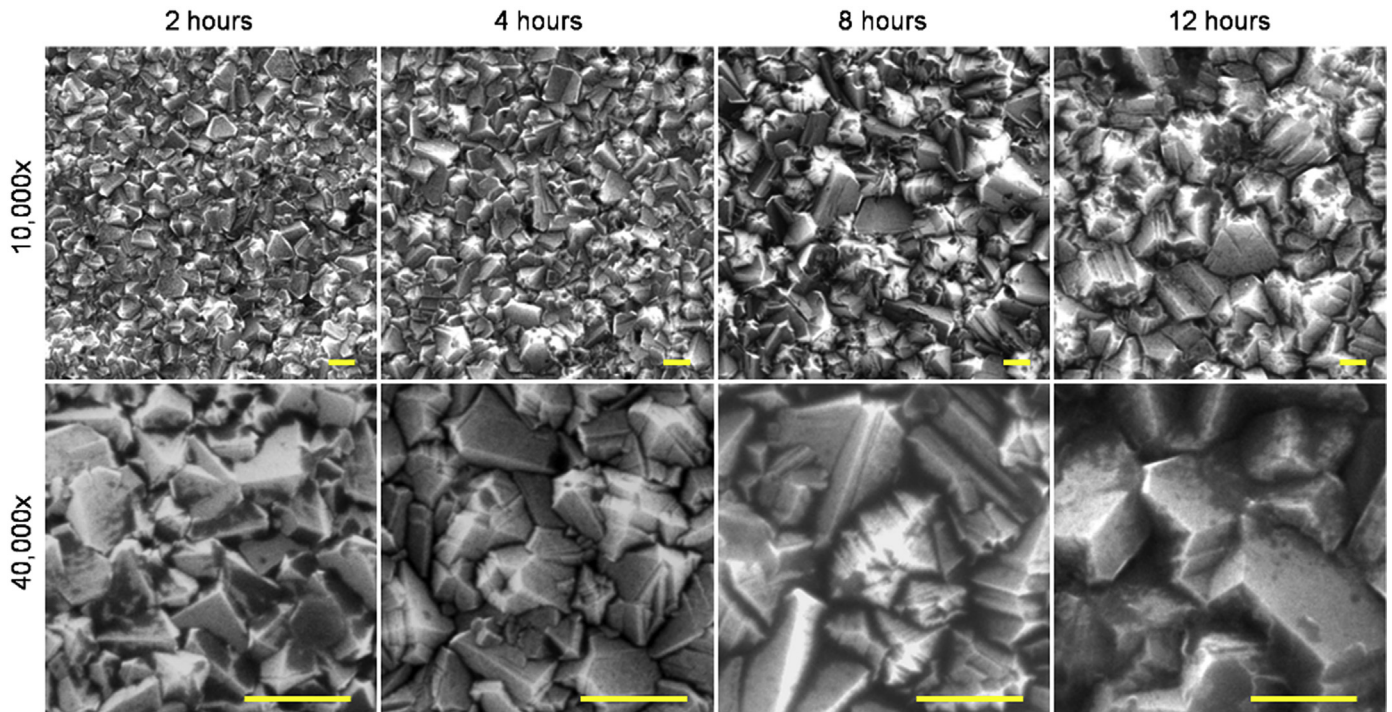


**Fig. 1.** SEM of diamond films grown on a silicon substrate. Diamond was deposited by CVD for 2, 4, 8 and 12 h, respectively. Representative SEM images at 10,000 × or 40,000 × magnification, respectively. Scale bars = 1 μm.

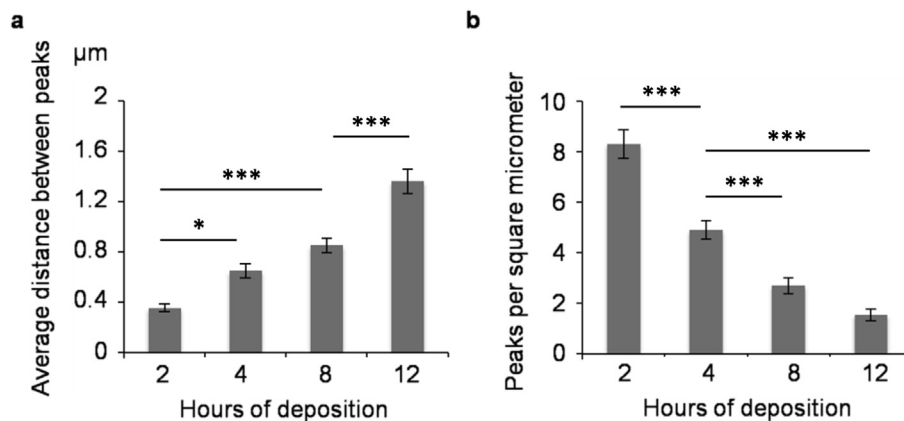


**Fig. 2.** Diamond crystal size quantification. a. Quantification of the average distance between the sharp peaks on two adjacent crystals. b. Quantification of the number of sharp peaks observed in a determined area (1 μm<sup>2</sup>). Values for (a) and (b) represent the average of 20 distances or areas, respectively, on 4 microscopic fields from 2 samples. Error bars = standard error of the mean, \**p* < 0.05, \*\*\**p* < 0.001.

cultured on truncated Vitronectin (VTN-N; LifeTechnologies, A14700) coated tissue-culture-treated dishes (Thermo-Fisher, 11844335) and passaged every 4–5 days with ethylenediaminetetraacetic acid (EDTA) (LifeTechnologies, 15575-020).

For neuronal differentiation, cells were cultured either in 12-well plates (Thermo-Fisher, 10098870), 6-well plates (Thermo-Fisher, 10119831) or on diamond substrates, coated either with the truncated form of vitronectin or with a combination of poly-L-ornithine 0.01% (Sigma–Aldrich, P4957-50 ML) and laminin 10 μg ml<sup>-1</sup> (Sigma–Aldrich, L2020-1 MG), each for 2 h at 37 °C. The medium used was either N2B27-R (rich) containing 1:1 Neurobasal (LifeTechnologies, 21103-049) and DMEM/F-12 with glutamax (LifeTechnologies, 31331-028), supplemented with: 1:100 B27 (LifeTechnologies, 17504-044), 1:200 N2 (LifeTechnologies, 17502-048), 5 μg ml<sup>-1</sup> insulin (Sigma–Aldrich, I 4011) glutamax 1 mM

(LifeTechnologies, 35050-038) (final glutamine concentration 2 mM), 1:100 nonessential amino acids (LifeTechnologies, 11140-035), 75 μM 2-mercaptoethanol (LifeTechnologies, 31350-010), 100 units ml<sup>-1</sup> penicillin and 100 μg ml<sup>-1</sup> streptomycin (Sigma–Aldrich, P4333), or N2B27-L (light) containing 1:1 Neurobasal and DMEM/F-12 with glutamax (final glutamine concentration 1 mM) supplemented with: 1:100 B27, 1:200 N2, 1:200 nonessential amino acids, 75 μM 2-mercaptoethanol, 100 units ml<sup>-1</sup> penicillin and 100 μg ml<sup>-1</sup> streptomycin. Cells were maintained at 37 °C in a humidified atmosphere containing 5% CO<sub>2</sub>.

We set out to generate a protocol for neuronal differentiation from hIPSCs and hESCs starting from cells cultured in Essential 8 (E8) medium. Our differentiation protocol is one in which the instructive cues are absent, allowing for a “default differentiation”, which could be later used as a starting point for the generation of specific

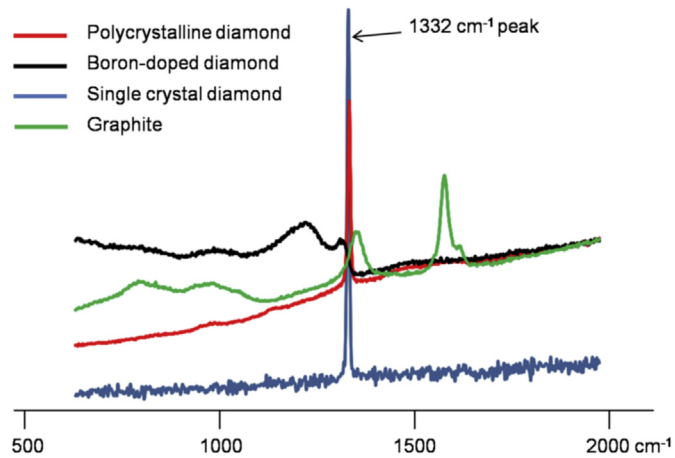


**Fig. 3.** Raman spectra showing the characteristic band shift for undoped (red) and B-doped (black) diamond grown on a silicon substrate compared to controls: single-crystal commercial diamond (blue) and graphite (green). (For interpretation of the references to colour in this figure legend, the reader is referred to the web version of this article.)

neuronal subtypes. First, we observed that pluripotent cells maintained in E8 medium proliferate faster than those maintained in KOSR, and that this fast rate continues for a few days after E8 has been removed. For this reason, the initial cell density had to be lowered (compared to the ones recommended in KOSR protocols) [29–31]. Pluripotent cells were passaged as usual on VTN-N-coated tissue-culture-treated plates and grown in E8 medium up to a confluency of 40–80%, depending on cell line. At this point, differentiation was started by changing the medium to N2B27-R (schematic diagram Fig. 4a). To block differentiation towards non-neural fates we employed the dual SMAD inhibition by the small molecules SB/LDN combination (SB431542 10  $\mu$ M (Tocris, 1614) and LDN193189 100 nM (Sigma–Aldrich, SML0559)) for the first 10–12 days. After that time, differentiating cells continued to be cultured in N2B27-R medium without inhibitors and passaged as required

(usually every 1–3 weeks) using Dispase on poly-L-ornithine/laminin-coated tissue-culture treated dishes. After 30–40 days, when obvious neuronal cells with neurites became predominant, Dispase was replaced by Accutase as the enzyme of choice for cell dissociation. Between days 50–70, cells underwent the final passage onto diamond.

Cells were dissociated either with Dispase II (Sigma–Aldrich, D4693) or StemPro® Accutase® (Life-Technologies, A11105-01) according to manufacturer instructions.

#### 2.4. Immunocytochemistry

Cells were fixed at the appropriate time points with 4%(wt/vol) paraformaldehyde in phosphate-buffered saline (PBS) with 1 mM calcium chloride for 20 min. Cells were blocked in a solution containing 5% normal serum (of the species in which the secondary antibody was raised), 1% BSA and 0.3% Triton X in PBS. Primary antibodies: glial fibrillary acidic protein (GFAP; Dako, Z0334), postsynaptic density protein 95 (PSD95; Abcam, AB18258), vesicular glutamate transporter 1 (vGlut1; Synaptic Systems, 135303), gamma-aminobutyric acid (GABA; Sigma–Aldrich A2052), tubulin  $\beta$ III (TuJ1; Covance, MMS-435P), and cleaved Caspase 3 (Cell Signalling, 9661). Secondary antibodies – all Alexa Fluor® (Life Technologies): 568 donkey anti-rabbit IgG (A10042), 488 donkey anti-mouse IgG (A-21202), 488 goat anti-mouse IgG<sub>1</sub> (A-21121) and 594 goat anti-mouse IgG<sub>2a</sub> (A-21135). All steps were performed at room temperature except for cleaved Caspase 3 which was incubated overnight at 4 °C. Images were taken using a Leica SP8 confocal system. For each field between 4 and 10 stacked images were obtained and the maximum projection was used for analysis.

#### 2.5. Quantification

For assessment of the diamond crystal structure either the distance between the sharp peaks of two adjacent crystals, or the number of sharp peaks observed in an area of 1  $\mu$ m<sup>2</sup> were assessed using ImageJ software version 1.49b. Each data point represents 20 distances or areas measured on four different SEM fields from two

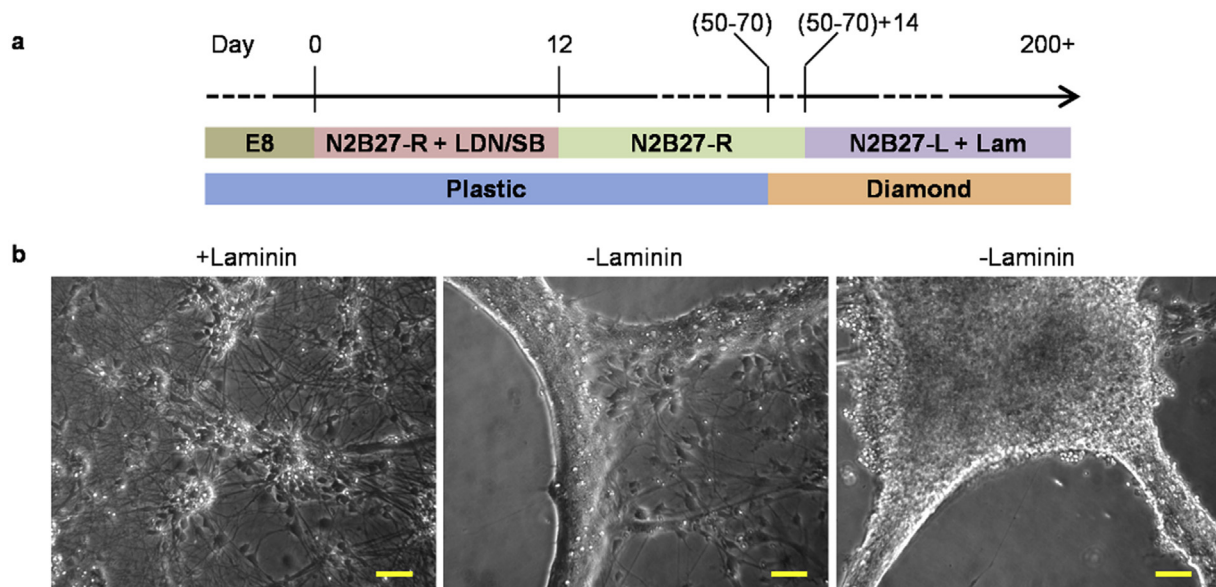


**Fig. 4.** Protocol for human neuronal differentiation on diamond. a. Schematics of the protocol. b. Phase-contrast microscopy of pluripotent-derived neural cells cultured on single-crystal diamond for more than 30 days. In the absence of laminin, the monolayer starts retracting (middle panel) until a clump of cells is formed (right panel). Scale bars = 50  $\mu$ m.

samples.

For immunofluorescence quantification the percentages of marker-positive cells were determined in samples derived from three independent experiments. The decision to image a specific field was made exclusively on the presence of nuclei; for each image the number of Hoechst-positive nuclei was assessed first, then the number of cells expressing the marker of interest was counted. The quantification of the area devoid of neurites was assessed in ImageJ as the sum area of the particles with background intensity signal. Each data point represents at least 6 fields.

The statistical significance was determined using One-way ANOVA followed by a Tukey HSD *post hoc* test. For statistical analysis 'R' version 3.1.1 was used (The R foundation for Statistical Computing, 2014). All data are presented as mean  $\pm$  standard error of the mean.

## 2.6. Oxidative stress

Cell culture media were supplemented with hydrogen peroxide solution (Sigma, H1009). For this experiment the media formulation was the same as N2B27-L, except that Neurobasal and B27 were removed and replaced with DMEM/F-12 and N2, respectively, and 2-mercaptoethanol was reduced to 50  $\mu$ M. A dose curve indicated that cell exposure to 50  $\mu$ M of hydrogen peroxide for 24 h does not induce full-scale apoptosis in our cell types. Hydrogen peroxide was first diluted in water (Sigma–Aldrich W3500) to a concentration of 0.1 M and then in DMEM/F-12 to a concentration of 1 mM. This working solution was applied to the cell media within 5 min from the first hydrogen peroxide dilution.

## 2.7. Electrophysiology

Patch clamp recordings of stem-cells grown onto a diamond scaffold were performed after more than 150 days in culture. The whole diamond scaffold was transferred into a submersion-style recording chamber. The cells were continuously perfused (2–3 ml/min) with HEPES Balanced Salt Solution (HBSS) containing 130 mM NaCl, 3 mM KCl, 10 mM 4-(2-hydroxyethyl)-1-piperazineethanesulfonic (HEPES)-free acid, 1 mM MgCl<sub>2</sub>, 2 mM CaCl<sub>2</sub> and 10 mM glucose, pH 7.3, 32 °C, 290–300 mOsm. Cells were visualized using infrared differential interference contrast microscopy (Olympus, BX51WI). Standard glass micropipettes of resistance 2.5–6 M $\Omega$  were used for recordings, filled with an internal solution containing: 145 mM K-gluconate, 5 mM NaCl, 10 mM HEPES-free acid, 0.2 mM EGTA, 0.3 mM Na-GTP, 4 mM Mg-ATP; pH 7.3; 280–290 mOsm. The liquid junction potential (JPC) that arose from the combination of bath and pipette solution was corrected for arithmetically.

All measurements were made using a Multiclamp 700B patch-clamp amplifier (Molecular Devices, USA). Data were low-pass filtered (5–10 kHz), digitised (100 kHz) and subsequently visualized and stored on a PC using pClamp electrophysiology software. Following entry into the whole-cell recording configuration, pipette capacitance was neutralized and the series resistance was compensated (10%–80% correction). Voltage-clamp (VC) recordings were made for the quantitative evaluation of voltage-gated currents; starting from a holding voltage of –82 mV, 12 voltage steps (10 mV for 30 ms) were applied and the consequent voltage-gated currents were measured. After VC recordings were completed, the amplifier was switched to  $I = 0$  pA current injection and the resting membrane potential (RMP) was assessed. Subsequent current-clamp (CC) recordings were performed to assess passive properties and eventual action-potential generation. These consisted in the application of 9 square-wave current pulses of 500 ms (–20, –10, 10, 20, 30, 40, 50, 60, 70 pA). Such recordings were

performed whilst keeping the pre-stimulus membrane voltage  $V_m$  at –67 mV with a constant current injection, in order to avoid biases arising from cell-to-cell variability in RMP.

## 2.8. Data analysis and statistics

For the characterization of the biophysical properties of voltage-gated outward current conductances (K<sup>+</sup> channels), *GV* curves were compiled for each cell by plotting specific conductance (nS/pF) vs test voltage. Data for both peak and steady-state plateau were acquired (Fig. 6A). Conductance density was used in order to account for cell-to-cell variability in size.  $G_{Max}$  and  $V_{1/2}$  values were calculated by single Boltzmann fits to the *GV* curve for each cell. For CC recordings, the input resistance ( $R_i$ ) was calculated using Ohm's law measuring the voltage deflection induced by a hyperpolarizing –20 pA, 500 ms current step. The change of input resistance ( $R_i$ ) upon increasing depolarization was represented by plotting the  $V_m$  deflection vs the relative injected current step. For both VC and CC recordings, data are presented in the format “mean  $\pm$  standard error of the mean (s.e.m.)”. A paired Student's *t*-test was used to compare  $G_{Max}$  and  $V_{1/2}$  at the peak and plateau.

## 3. Results

### 3.1. Diamond supports long term culture of human neurons

In the course of the neuronal differentiation protocol we observed that the polyornithine/laminin coating of the substrate was effective in maintaining cellular attachment to the substrate in the first stages of the protocol, when cells were passaged relatively frequently. However, during final neuronal differentiation it became difficult to maintain the monolayer attached to diamond long term (over 30 days). This problem was solved by supplementing the media with laminin (2  $\mu$ g ml<sup>–1</sup>) once a week (Fig. 4b). Furthermore, N2B27-R medium has a formulation very similar to the original N2B27 developed over 10 years ago for the neural differentiation of mouse ES cells [36]. Since mouse neural progenitors are highly proliferating cells, able to undergo terminal neuronal differentiation in just two weeks, we inferred that this particular formulation might not be ideally suited for long-term maintenance of human neurons. For this reason we developed a related medium (N2B27-L) with reduced levels of insulin, non-essential amino acids and glutamine. Two weeks after passage onto the diamond substrate the media was changed from N2B27-R to N2B27-L (Fig. 4a). This media modification allowed us to consistently culture neuronal cells on diamond past 200 days of differentiation.

During development, neural progenitors produce two major cell classes: neurons and glia. The choice between these two fates is temporally regulated by specific transcription factors; neurons being produced earlier and glia later [37]. The presence of glial cells in culture is required for the full maturation of neuronal cells [38], and the extended time of our protocol of over 150 days of differentiation allowed the generation of glia alongside neuronal cells. Staining for the neuronal specific form of tubulin (TuJ1) and for the glial fibrillary acidic protein (a type of intermediary filament expressed specifically in astrocytes) showed the two types of cells intermingled (Fig. 5).

### 3.2. Neuronal maturation on diamond substrates

Furthermore, we assessed the presence of synaptic markers in the differentiated neurons. In the human brain the majority of synapses are excitatory. PSD95 is a scaffold protein essential for the architecture of such synapses [39]. We found it to be ubiquitously

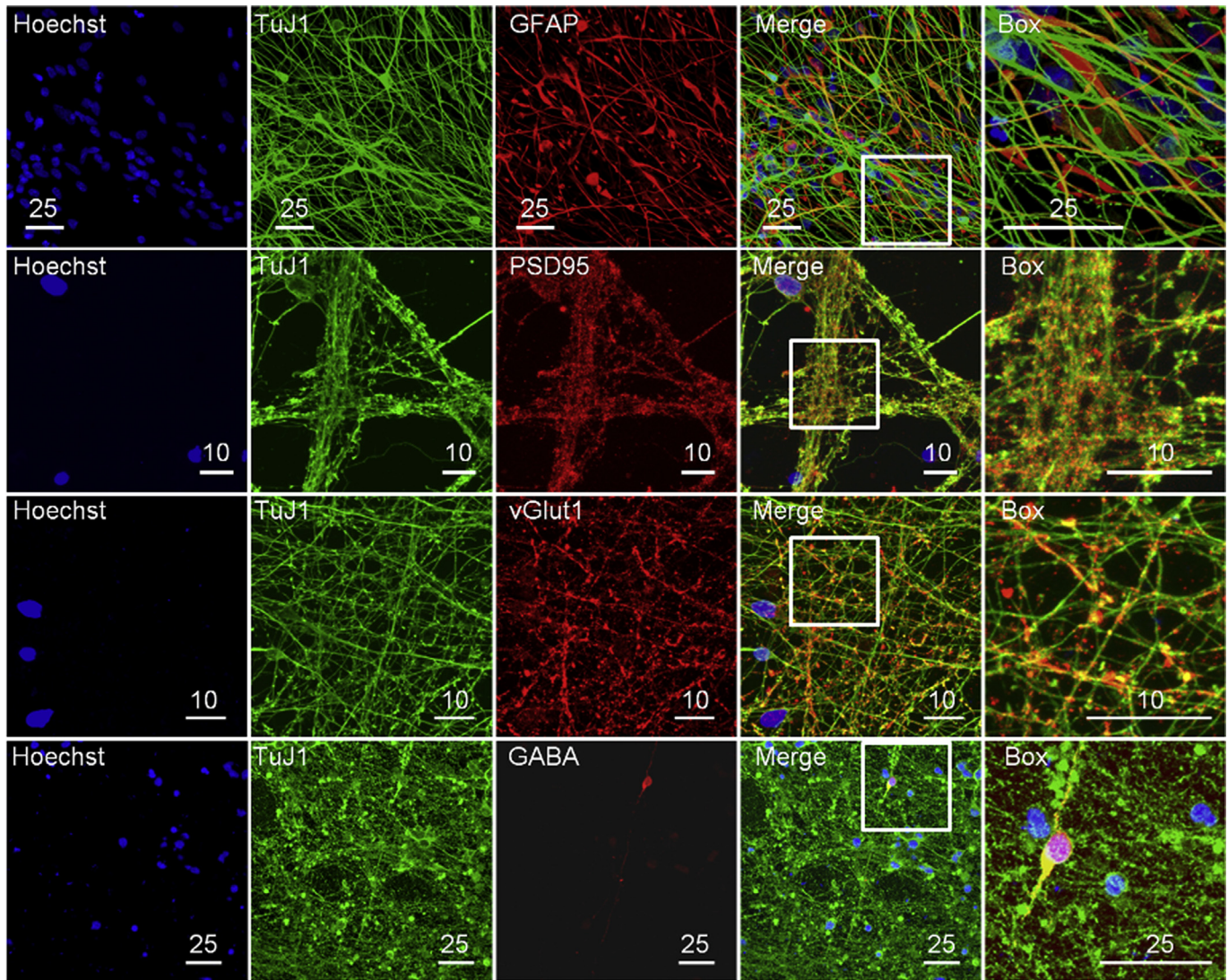


**Fig. 5.** Characterization of the neural population differentiated on diamond by the proposed protocol. Fluorescent microscopy of cells differentiated for more than 150 days stained blue for nuclei (Hoechst), green for tubulin  $\beta$ III (TuJ1) and red for glial fibrillary acidic protein (GFAP), postsynaptic density protein 95 (PSD95), vesicular glutamate transporter 1 (vGlut1) and gamma-aminobutyric acid (GABA), respectively. Scale bars = 10 or 25  $\mu$ m. (For interpretation of the references to colour in this figure legend, the reader is referred to the web version of this article.)

expressed as *punctae* associated with the TuJ1 filaments (Fig. 5). The clustering of PSD95 in *punctae* suggests that the protein is located at the synaptic level. Glutamate is the main neurotransmitter of excitatory synapses and two vesicular transporters for this molecule are active in the brain: vGlut1 and vGlut2. vGlut1 is mainly expressed in telencephalic regions [40]. We observed vGlut1 to be expressed in vesicles associated with the TuJ1 filaments (Fig. 5). In contrast, observation of neurons positive for GABA, the main inhibitory neurotransmitter of the mammalian central nervous system [41], represented a rare event (Fig. 5). Together, these data suggest that our protocol produces mature neurons forming mainly excitatory synapses belonging most likely to the neocortex. Additionally, the presence of rare GABAergic neurons indicates that these neuronal types could also be produced with minor modifications to the protocol.

The functional profile of neuronal stem cells grown on a diamond substrate was assessed by performing patch-clamp whole-cell recordings on two samples left to differentiate in culture for an extended period of time (over 150 days). Immediately after

entering whole-cell VC mode, the membrane capacitance was assessed and series resistance compensated for (10–80% correction). The application of 10 mV voltage steps revealed the presence of large outward  $K^+$  currents (including a fast inactivating peak and non-inactivating plateau). In the majority of cells the outward current was preceded by a fast, inward-going, presumably  $Na^+$  current (Fig. 6A–B). We focused our analysis on outward  $K^+$  currents as (i) these were present in all cells, and (ii) measurements of the very fast  $Na^+$  current were compromised by voltage-clamp issues (arising from the complex cellular geometry of mature neurons) and the effects of the rapidly following  $K^+$  currents. The increase of outward current density and conductance ( $G$ ) with increasing voltage depolarization followed a Boltzmann fit, both when measured at peak or at plateau (Fig. 6C). Cell-to-cell fit of the GV curve with a single Boltzmann function revealed a small but significant increase of the extrapolated  $K^+$   $G_{Max}$  density of the peak vs the plateau ( $n = 26$ ; Peak:  $0.497 \text{ nS/pF} \pm 0.06 \text{ nS/pF}$  vs Plateau:  $0.436 \text{ nS/pF} \pm 0.05 \text{ nS/pF}$ , paired t-test  $p = 0.001$ ; Fig. 6D) but no difference was observed in  $V_{1/2}$  (Peak:  $-15.5 \text{ mV} \pm 1.6 \text{ mV}$  vs

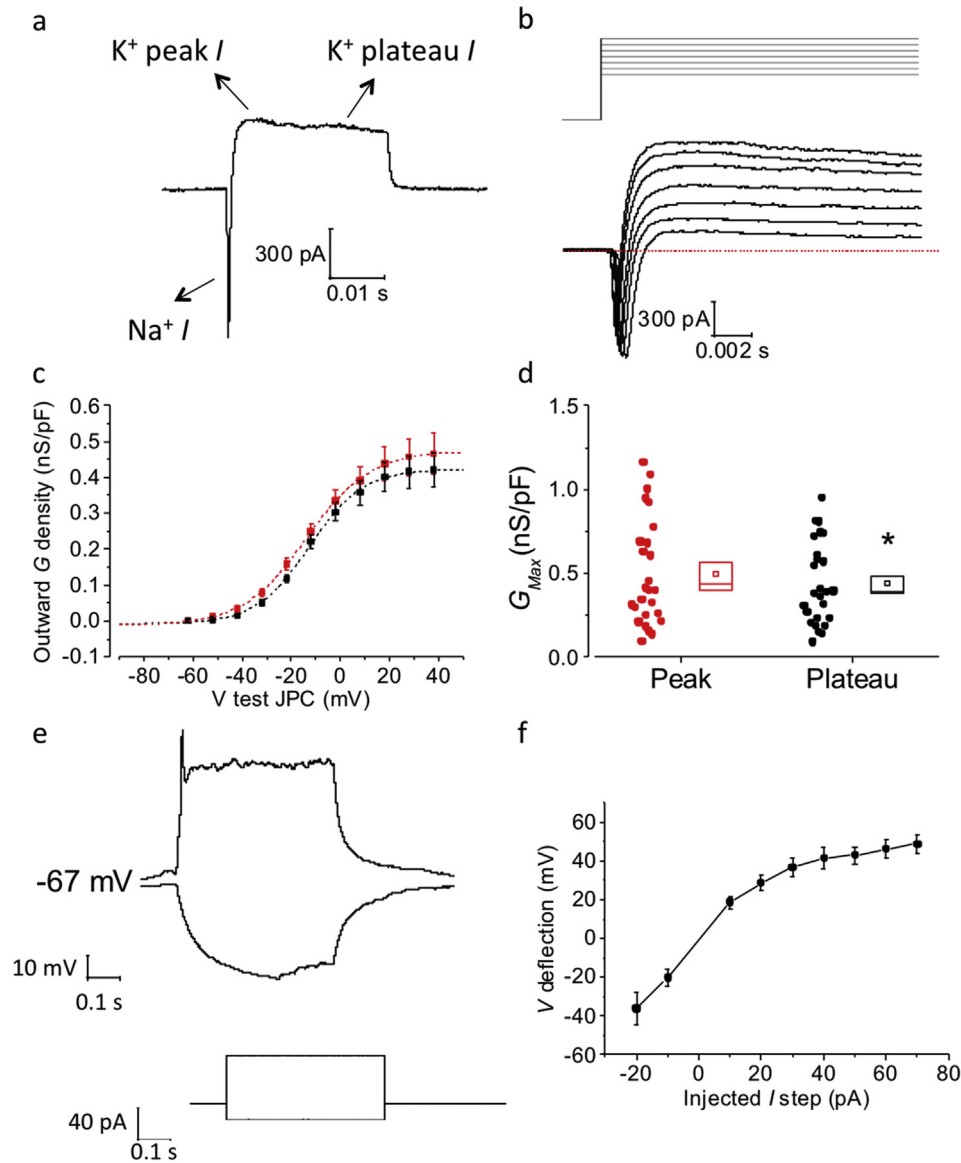


**Fig. 6.** Electrophysiological characterization of neural differentiation on a diamond substrate. The cells were differentiated for more than 150 days before performing whole-cell patch-clamp recordings. a–b) The application of successive voltage steps in VC, starting from a  $V_m = -82$  mV, resulted in the generation of a negative inward ( $\text{Na}^+$ ) and positive ( $\text{K}^+$ ) outward current ( $I$ ); the latter one included an initial peak and a subsequent steady-state plateau. c) The GV curve of outward voltage-gated currents, which followed a single-Boltzmann fit, was compiled for both the initial peak (red) and the plateau (black). d) Each cell-to-cell Boltzmann fit of single GV curves allowed us to estimate the  $G_{\text{max}}$  of both peak and plateau outward  $\text{K}^+$  voltage-gated conductances; the dots represent the value measured for each cell, while the box on the right includes a representation of the mean (small square), 1 s.e.m. boundaries (upper and lower line) and the median (middle line). e) CC recordings consisting of the injection of hyperpolarizing and depolarizing 500 ms current-steps, allowed us to measure the  $R_i$  and eventual spike-like events as a consequence of  $V_m$  hyper- and de-polarization. f) The voltage deflection was plotted vs the injected current for 7 cells, showing a linear increase at lower  $V_m$  but a progressive reduction of the slope as the cell gets more depolarized. This is mostly due to the activation of voltage-gated  $\text{K}^+$  conductances upon depolarization. (For interpretation of the references to colour in this figure legend, the reader is referred to the web version of this article.)

Plateau:  $-13.9$  mV  $\pm$  1.3 mV, paired t-test  $p = 0.2$ ; not shown).

In current-clamp measurements, the average RMP and  $R_i$  of these cells was  $-49.9$  mV  $\pm$  3.1 mV and  $1.07 \pm 0.04$  G $\Omega$ , respectively. An example of the response to current injection is shown in Fig. 6E. In accordance with the voltage-clamp data above, input resistance decreased as the cells were increasingly depolarized using incrementally large current injections, as illustrated by Fig. 6F which plots steady-state voltage response vs injected current for 7 cells resting at  $\sim -67$  mV.

### 3.3. Neurite density depends on diamond microstructure

At this point we assessed the relationship between the neurons

produced and the diamond surface characteristics. One line of investigation concerned the roughness of the surface on which cells were cultured. For this purpose we compared a commercial smooth-polished diamond surface with in-house produced polycrystalline, unpolished diamond of various roughnesses, as shown in Fig. 1 and Suppl. Fig. 2. The second line of investigation assessed the effect of the presence of the boron dopant.

First, we ascertained that all substrates tested could support differentiation and long-term survival of human neurons and glial cells (Fig. 7). In all conditions, highly dense neurite formation was observed, forming multiple connections between the cell bodies. However, for certain substrates, most notably for polished diamond and for the diamond films with longer deposition times, there were

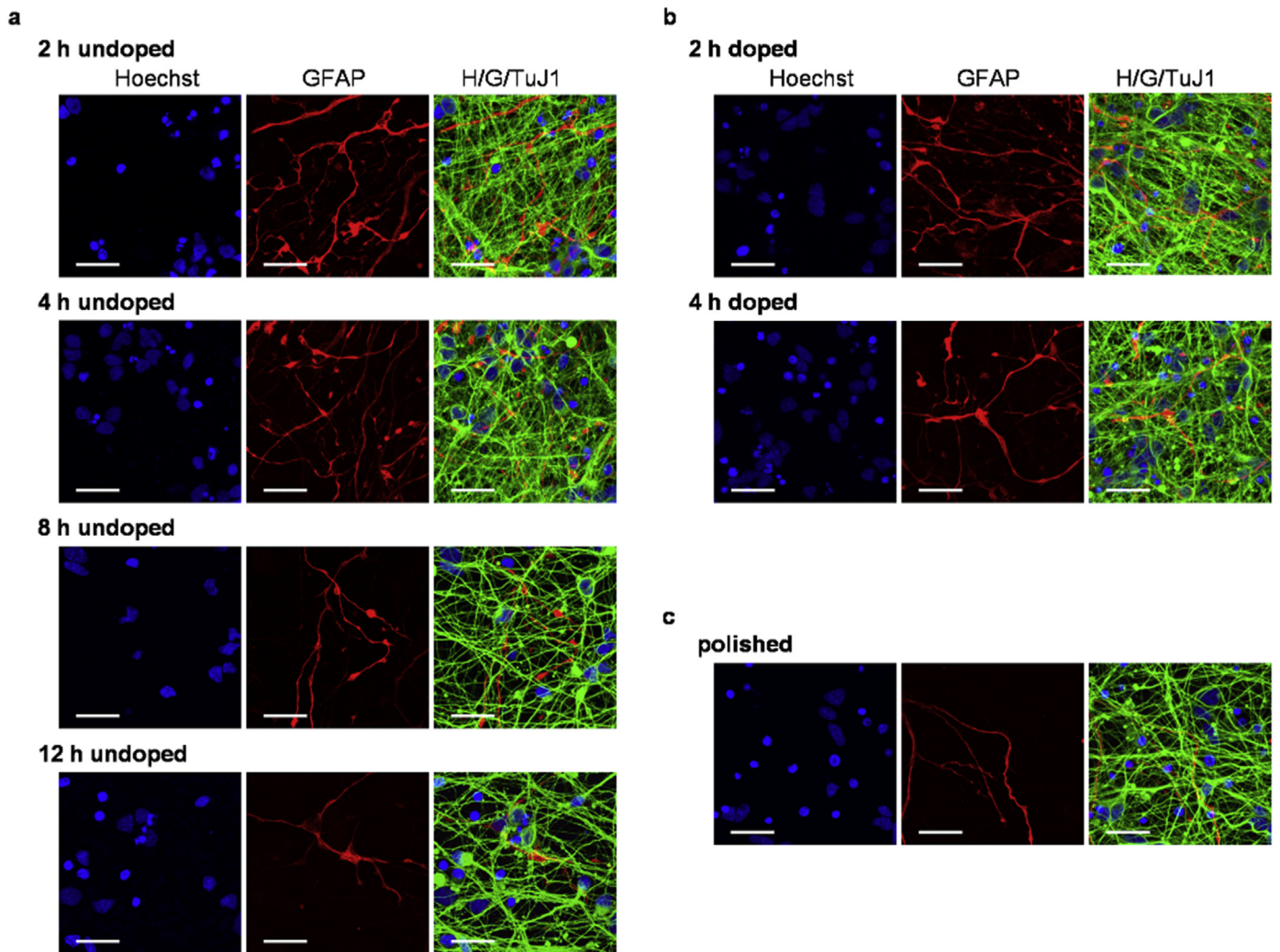


**Fig. 7.** Characterization of neural differentiation on various diamond substrates. Immunofluorescence of cells differentiated for more than 150 days stained blue for nuclei (Hoechst), green for tubulin  $\beta$ III (TuJ1) and red for glial fibrillary acidic protein (GFAP). Scale bars = 25  $\mu$ m. a. Undoped diamond films grown on silicon substrate for 2, 4, 8 and 12 h, respectively. b. Boron-doped diamond films grown on silicon substrate for 2 and 4 h, respectively. c. commercial polished undoped diamond. (For interpretation of the references to colour in this figure legend, the reader is referred to the web version of this article.)

areas with few or no neurites. When these were quantified by measuring the sum of all the areas free of neurites on a particular microscopic field, we found that the area devoid of neurites increased with increasing deposition time and hence the diamond crystal size. A significant difference was observed between the substrates with the smallest crystals (grown for 2 and 4 h) either undoped or doped, compared to the undoped substrate grown for 12 h (Fig. 8a). In the case of polished diamond, the surface of the area devoid of neurites was between that seen with small and large diamond crystals, and no statistically significant difference could be calculated with any of the other conditions. When the cell number was assessed we observed a similar general trend: namely the surface with the largest crystals had the lowest number of cells although no significant difference was seen between different conditions (Fig. 8b). Together these data indicate that from the conditions tested, polycrystalline diamond with smaller crystallites (*i.e.* with no more than 1  $\mu$ m average distance between peaks) is the optimal substrate for the differentiation of human neural progenitors. This is consistent with previous work [15,18], which showed that small-grained ultrananocrystalline diamond promotes neuronal attachment and outgrowth.

#### 3.4. Presence of boron as a dopant does not affect cell survival

Comparing the size and number of neurons grown on undoped and boron-doped diamond we found that boron-doped diamond has no adverse influence on cell survival and neurite formation. However, this does not preclude the possibility that boron induces some level of apoptosis, which is compensated in long-term culture by cell proliferation. To check for this we tested for the presence of Caspase 3, which is an “executioner” caspase in the apoptotic pathway activated by proteolytic cleavage [42]. In differentiated cells stained for the activated form (cleaved Caspase 3) we did not observe a difference between the apoptosis levels of cells grown on undoped *versus* doped diamond. Furthermore, we challenged the cells with 24-h oxidative stress conditions with hydrogen peroxide, a test routinely used in neuroscience research. Hydrogen peroxide significantly increased the apoptosis levels compared to control conditions, but again no difference was observed between the undoped and doped diamond (Fig. 9), indicating that boron doping, at least at the levels used by us, does not have an apoptotic inducing effect on these types of cells.

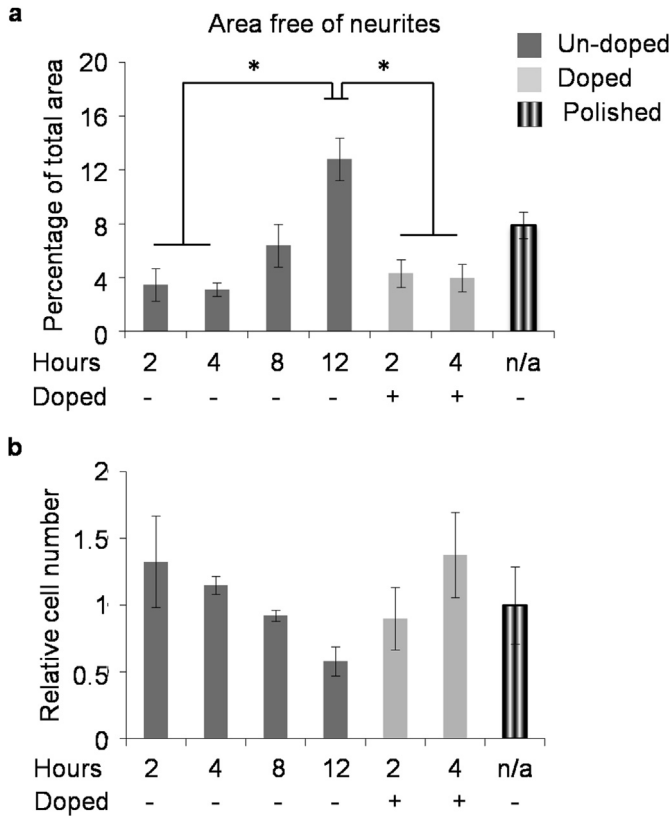


**Fig. 8.** Quantification of neuronal growth on various diamond substrates. a. Quantification of the percentage of area devoided of neurites for each type of substrate. b. Quantification of the total number of cell nuclei present for each type of substrate. The data for the control substrate (polished undoped diamond) has been arbitrarily set to 1. Each data point represents the average of three experiments. Error bars = standard error of the mean, \**p* < 0.05.

#### 4. Discussion

We have presented a protocol for undirected neuronal differentiation of human pluripotent cells on diamond substrates, where they can be maintained for long-term culture. The differentiated cells present the indicators of a mature culture with a mixture of neurons and astrocytes. The neurons display mature synaptic markers, clustered in vesicles. The functional characterization of these cells revealed that they develop the fast voltage-gated inward Na<sup>+</sup> currents and outward voltage-gated K<sup>+</sup> currents which are prerequisite for regenerative action-potential genesis in vertebrate neurons. The neurons also exhibit a negative RMP within the range found in mammalian nerve cells. These data, along with the molecular-marker characterization, reveal that diamond scaffolds are compatible with the development of pluripotent stem cells into more mature neuron-like cells.

We show that the presented method can efficiently produce neurons on all substrates tested and provide evidence for polycrystalline diamond with small crystals being the optimal substrate for our purposes. Boron doping of diamond does not adversely affect the culture, either in cell number, neurite formation or apoptosis levels, during basal or stress conditions.

A striking observation derived from this study is that the efficiency of neurite formation is significantly reduced once the average distance between most conspicuous surface features exceeds 1 μm. This has implications not only on future design of diamond surfaces for neuro-research, but also on the design of electrodes for diamond microarrays. Since the current available methods make it challenging to produce diamond electrodes much smaller than 1 μm, another solution, which could be explored, is to space the electrodes at distances exceeding a few times the size of a cell body.

Furthermore, our study pioneers neural differentiation from human pluripotent stem cells maintained in xeno-free, fully defined conditions. This is a trend that will only be accentuated in the coming years, demanded by the need to remove animal contaminants and increase consistency in cell therapy experiments. However, it has to be pointed out that the differentiation process

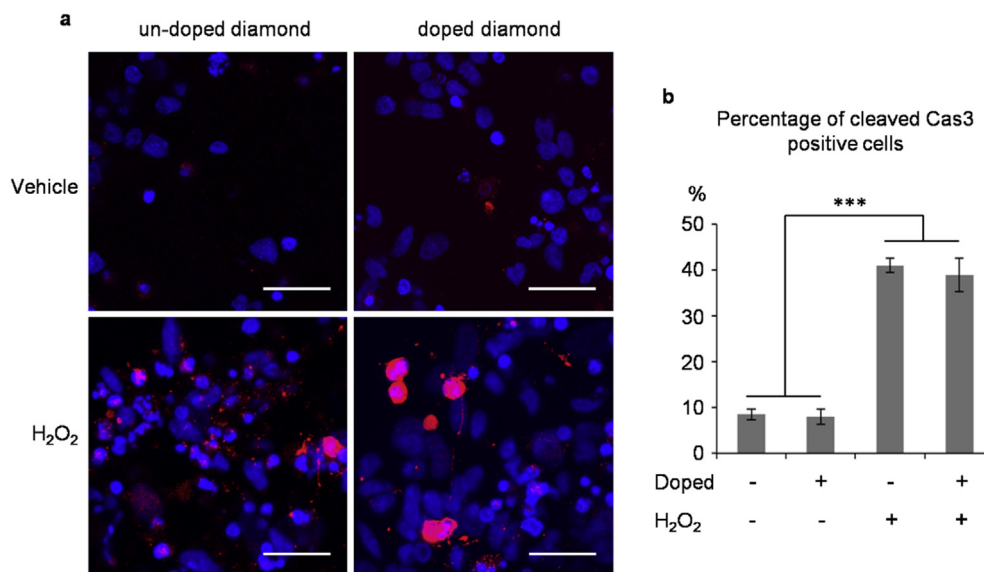


**Fig. 9.** Oxidative stress challenge of neuronal cells grown on diamond. a. Immunofluorescence of cells treated for 24 h with H<sub>2</sub>O<sub>2</sub> 50 μM or vehicle and stained blue for nuclei (Hoechst) and red for cleaved caspase 3. Cells were differentiated on either undoped or boron-doped diamond grown on a silicon substrate for 4 h. Scale bars = 25 μm. b. Quantification of the percentage of cells positive for cleaved caspase 3. Each data point represents the average of three experiments. Error bars = standard error of the mean, \*\*\**p* < 0.001. (For interpretation of the references to colour in this figure legend, the reader is referred to the web version of this article.)

itself employed was not xeno-free as both the supplements used here (B27 and N2) contained BSA. To date, we are not aware of any neuronal differentiation performed in xeno-free conditions. Such an attempt, in the future, will either have to replace the bovine albumin with human one, or dispense with it altogether, as in the case of E8 medium for pluripotent cells. Removing albumin from the medium will be more challenging for neuronal cells than for pluripotent cells considering the long differentiation procedure and the particular sensitivity of human neural cells. On the other hand, human albumin is a very expensive alternative and a limited resource.

## 5. Conclusions

Diamond is a suitable substrate for long-term culture of human neurons and boron doping does not adversely affect its role as a cellular substrate. Following our protocol, mature electrically active neurons can be maintained and studied. This work provides a platform towards a diamond MEA for the study of human neuronal circuits.

## Acknowledgements

The authors thank Dr. James Smith for outstanding technical support with Carbon Vapour Deposition and Raman Spectroscopy and Dr. Tilo Kunath for the kind gift of NAS2 IPS cell line. The confocal microscopy and scanning electron microscopy was performed at the Wolfson Imaging Facility, Medical Sciences Building, University of Bristol.

This work was funded by EPSRC (grant number: EP/K002503/1).

The funders had no role in study design, data collection and analysis, decision to publish, or preparation of the manuscript.

## Appendix A. Supplementary data

Raw data on which this paper is based can be accessed via the University of Bristol data repository. <http://dx.doi.org/10.5523/bris.796g35j4kg9r1toefvi82qxxf>.

Supplementary data related to this article can be found at <http://dx.doi.org/10.1016/j.biomaterials.2015.04.050>.

## References

- E.M. Regan, A. Taylor, J.B. Uney, A.D. Dick, P.W. May, J.P. McGeehan, Spatially controlling neuronal adhesion and inflammation reactions on implantable diamond, *IEEE J. Emerg. Sel. Top. Circuits Syst.* 1 (2011) 557–565, <http://dx.doi.org/10.1109/jtcas.2011.2174469>.
- P.W. May, E.M. Regan, A. Taylor, J. Uney, A.D. Dick, J. McGeehan, Spatially controlling neuronal adhesion on CVD diamond, *Diam. Relat. Mater.* 23 (2012) 100–104, <http://dx.doi.org/10.1016/j.diamond.2012.01.023>.
- C. Hébert, J. Warnking, A. Depaulis, L.A. Garçon, M. Mermoux, D. Eon, et al., Microfabrication, characterization and in vivo MRI compatibility of diamond microelectrodes array for neural interfacing, *Mat. Sci. Eng. C* 46 (2015) 25–31, <http://dx.doi.org/10.1016/j.msec.2014.10.018>.
- P.W. May, Diamond thin films: a 21st-century material, *Philos. Trans. R. Soc. A Math. Phys. Eng. Sci.* 358 (2000) 473–495, <http://dx.doi.org/10.1098/rsta.2000.0542>.
- P.W. May, The New Diamond Age? *Science* 319 (2008) 1490–1491, <http://dx.doi.org/10.1126/science.1154949>.
- L.A. Thomson, F.C. Law, N. Rushton, J. Franks, Biocompatibility of diamond-like carbon coating, *Biomaterials* 12 (1991) 37–40, [http://dx.doi.org/10.1016/0142-9612\(91\)90129-X](http://dx.doi.org/10.1016/0142-9612(91)90129-X).
- L. Tang, C. Tsai, W.W. Gerberich, L. Kruckeberg, D.R. Kania, Biocompatibility of chemical-vapour-deposited diamond, *Biomaterials* 16 (1995) 483–488, [http://dx.doi.org/10.1016/0142-9612\(95\)98822-V](http://dx.doi.org/10.1016/0142-9612(95)98822-V).
- M. Jones, I. McColl, D. Grant, K. Parker, T. Parker, Haemocompatibility of DLC and TiC–TiN interlayers on titanium, *Diam. Relat. Mater.* 8 (1999) 457–462, [http://dx.doi.org/10.1016/S0925-9635\(98\)00426-9](http://dx.doi.org/10.1016/S0925-9635(98)00426-9).
- M. Allen, B. Myer, N. Rushton, In vitro and in vivo investigations into the biocompatibility of diamond-like carbon (DLC) coatings for orthopedic applications, *J. Biomed. Mater. Res.* 58 (2001) 319–328, [10.1002/1097-4636\(2001\)58:3<319::AID-JBM1024>3.0.CO;2-F](http://dx.doi.org/10.1002/1097-4636(2001)58:3<319::AID-JBM1024>3.0.CO;2-F).
- N. Nurdin, P. François, Y. Mugnier, J. Krumeich, M. Moret, B.O. Aronsson, et al., Haemocompatibility evaluation of DLC- and SiC-coated surfaces, *Eur. Cells Mater.* 5 (2003) 17–28.
- A. Kraft, Doped diamond: a compact review on a new, versatile electrode material, *Int. J. Electrochem. Sci.* 2 (2007) 355–385, <http://dx.doi.org/10.1242/jeb.00516>.
- J. Roeser, N.F.A. Alting, H.P. Permentier, A.P. Bruins, R. Bischoff, Boron-doped diamond electrodes for the electrochemical oxidation and cleavage of peptides, *Anal. Chem.* 85 (2013) 6626–6632, <http://dx.doi.org/10.1021/ac303795c>.
- C.G. Specht, O.A. Williams, R.B. Jackman, R. Schoepfer, Ordered growth of neurons on diamond, *Biomaterials* 25 (2004) 4073–4078, <http://dx.doi.org/10.1016/j.biomaterials.2003.11.006>.
- Y.-C. Chen, D.-C. Lee, C.-Y. Hsiao, Y.-F. Chung, H.-C. Chen, J.P. Thomas, et al., The effect of ultra-nanocrystalline diamond films on the proliferation and differentiation of neural stem cells, *Biomaterials* 30 (2009) 3428–3435, <http://dx.doi.org/10.1016/j.biomaterials.2009.03.058>.
- Y.-C. Chen, D.-C. Lee, T.-Y. Tsai, C.-Y. Hsiao, J.-W. Liu, C.-Y. Kao, et al., Induction and regulation of differentiation in neural stem cells on ultra-nanocrystalline diamond films, *Biomaterials* 31 (2010) 5575–5587, <http://dx.doi.org/10.1016/j.biomaterials.2010.03.061>.
- E.M. Regan, J.B. Uney, A.D. Dick, Y. Zhang, J. Nunez-Yanez, J.P. McGeehan, et al., Differential patterning of neuronal, glial and neural progenitor cells on phosphorus-doped and UV irradiated diamond-like carbon, *Biomaterials* 31 (2010) 207–215, <http://dx.doi.org/10.1016/j.biomaterials.2009.09.042>.
- A. Bendali, C. Agnès, S. Meffert, V. Forster, A. Bongrain, J.C. Arnault, et al., Distinctive glial and neuronal interfacing on nanocrystalline diamond, *PLoS One* 9 (2014), <http://dx.doi.org/10.1371/journal.pone.0092562>.
- A. Thalhammer, R.J. Edgington, L.A. Cingolani, R. Schoepfer, R.B. Jackman, The use of nanodiamond monolayer coatings to promote the formation of functional neuronal networks, *Biomaterials* 31 (2010) 2097–2104, <http://dx.doi.org/10.1016/j.biomaterials.2009.11.109>.
- A. Ahnood, M.C. Escudie, R. Cicione, C.D. Abeyrathne, K. Ganesan, K.E. Fox, et al., Ultrananocrystalline diamond-CMOS device integration route for high acuity retinal prostheses, *Biomed. Microdevices* 17 (2015) 50, <http://dx.doi.org/10.1007/s10544-015-9952-y>.
- D.J. Garrett, A.L. Saunders, C. McGowan, J. Specks, K. Ganesan, H. Meffin, et al., In vivo biocompatibility of boron doped and nitrogen included conductive-diamond for use in medical implants, *J. Biomed. Mater. Res. B Appl. Biomater.* (2015), <http://dx.doi.org/10.1002/jbm.b.33331>.
- R.E. Chapin, W.W. Ku, The reproductive toxicity of boric acid, *Environ. Health Perspect.* 102 (Suppl.:87–91) (1994), <http://dx.doi.org/10.1289/ehp.94102s787>.
- R.E. Chapin, W.W. Ku, M.A. Kenney, H. McCoy, B. Gladen, R.N. Wine, et al., The effects of dietary boron on bone strength in rats, *Fundam. Appl. Toxicol.* 35 (1997) 205–215 doi:S0272059096922757 [pii].
- W.A. Robbins, L. Xun, J. Jia, N. Kennedy, D.A. Elashoff, L. Ping, Chronic boron exposure and human semen parameters, *Reprod. Toxicol.* 29 (2010) 184–190, <http://dx.doi.org/10.1016/j.reprotox.2009.11.003>.
- N. Başaran, Y. Duydu, H.M. Bolt, Reproductive toxicity in boron exposed workers in Bandirma, *Turk. J. Trace Elem. Med. Biol.* 26 (2012) 165–167, <http://dx.doi.org/10.1016/j.jtemb.2012.04.013>.
- M.A. Soriano-Ursúa, E.D. Farfán-García, Y. López-Cabrera, E. Querejeta, J.G. Trujillo-Ferrara, Boron-containing acids: preliminary evaluation of acute toxicity and access to the brain determined by Raman scattering spectroscopy, *Neurotoxicology* 40 (2014) 8–15, <http://dx.doi.org/10.1016/j.neuro.2013.10.005>.
- L. Horváth, A. Magrez, D. Golberg, C. Zhi, Y. Bando, R. Smajda, et al., In vitro investigation of the cellular toxicity of boron nitride nanotubes, *ACS Nano* 5 (2011) 3800–3810, <http://dx.doi.org/10.1021/nn200139h>.
- P.W. May, W.J. Ludlow, M. Hannaway, P.J. Heard, J.A. Smith, K.N. Rosser, Raman and conductivity studies of boron-doped microcrystalline diamond, faceted nanocrystalline diamond and cauliflower diamond films, *Diam. Relat. Mater.* 17 (2008) 105–117, <http://dx.doi.org/10.1016/j.diamond.2007.11.005>.
- N.G. Ferreira, L.L.G. Silva, E.J. Corat, V.J. Trava-Airoldi, K. Iha, Electrochemical characterization on semiconductors p-type CVD diamond electrodes, *Braz. J. Phys.* 29 (1999) 760–763, <http://dx.doi.org/10.1590/s0103-97331999000400030>.
- S.M. Chambers, C.A. Fasano, E.P. Papapetrou, M. Tomishima, M. Sadelain, L. Studer, Highly efficient neural conversion of human ES and iPS cells by dual inhibition of SMAD signaling, *Nat. Biotechnol.* 27 (2009) 275–280, <http://dx.doi.org/10.1038/nbt0509-485a>.
- S.M. Chambers, Y. Qi, Y. Mica, G. Lee, X.-J. Zhang, L. Niu, et al., Combined small-molecule inhibition accelerates developmental timing and converts human pluripotent stem cells into nociceptors, *Nat. Biotechnol.* 30 (2012) 715–720, <http://dx.doi.org/10.1038/nbt.2249>.
- Y. Shi, P. Kirwan, J. Smith, H.P.C. Robinson, F.J. Livesey, Human cerebral cortex development from pluripotent stem cells to functional excitatory synapses, *Nat. Neurosci.* 15 (2012) 477–486, <http://dx.doi.org/10.1038/nn.3041>.
- N. Sun, N.J. Panetta, D.M. Gupta, K.D. Wilson, A. Lee, F. Jia, et al., Feeder-free derivation of induced pluripotent stem cells from adult human adipose stem cells, *Proc. Natl. Acad. Sci. U. S. A.* 106 (2009) 15720–15725, <http://dx.doi.org/10.1073/pnas.0908450106>.
- G. Chen, D.R. Gulbranson, Z. Hou, J.M. Bolin, V. Ruotti, M.D. Probasco, et al.,

- Chemically defined conditions for human iPSC derivation and culture, *Nat. Methods* 8 (2011) 424–429, <http://dx.doi.org/10.1038/nmeth.1593>.
- [34] M. Nakagawa, Y. Taniguchi, S. Senda, N. Takizawa, T. Ichisaka, K. Asano, et al., A novel efficient feeder-free culture system for the derivation of human induced pluripotent stem cells, *Sci. Rep.* 4 (2014) 3594, <http://dx.doi.org/10.1038/srep03594>.
- [35] M.J. Devine, M. Rytten, P. Vodicka, A.J. Thomson, T. Burdon, H. Houlden, et al., Parkinson's disease induced pluripotent stem cells with triplication of the  $\alpha$ -synuclein locus, *Nat. Commun.* 2 (2011) 440, <http://dx.doi.org/10.1038/ncomms1453>.
- [36] Q.-L. Ying, M. Stavridis, D. Griffiths, M. Li, A. Smith, Conversion of embryonic stem cells into neuroectodermal precursors in adherent monoculture, vol. 21, 2003, <http://dx.doi.org/10.1038/nbt780>.
- [37] M. Nieto, C. Schuurmans, O. Britz, F. Guillemot, Neural bHLH genes control the neuronal versus glial fate decision in cortical progenitors, *Neuron* 29 (2001) 401–413, [http://dx.doi.org/10.1016/S0896-6273\(01\)00214-8](http://dx.doi.org/10.1016/S0896-6273(01)00214-8).
- [38] M. Pyka, C. Busse, C. Seidenbecher, E.D. Gundelfinger, A. Faissner, Astrocytes are crucial for survival and maturation of embryonic hippocampal neurons in a neuron-glia cell-insert coculture assay, *Synapse* 65 (2011) 41–53, <http://dx.doi.org/10.1002/syn.20816>.
- [39] H. Cline, Synaptogenesis: A balancing act between excitation and inhibition, *Curr. Biol.* 15 (2005), <http://dx.doi.org/10.1016/j.cub.2005.03.010>.
- [40] T. Kaneko, F. Fujiyama, Complementary distribution of vesicular glutamate transporters in the central nervous system, *Neurosci. Res.* 42 (2002) 243–250, [http://dx.doi.org/10.1016/S0168-0102\(02\)00009-3](http://dx.doi.org/10.1016/S0168-0102(02)00009-3).
- [41] D.F. Owens, A.R. Kriegstein, Is there more to GABA than synaptic inhibition? *Nat. Rev. Neurosci.* 3 (2002) 715–727, <http://dx.doi.org/10.1038/nrn919>.
- [42] K.M. Boatright, G.S. Salvesen, Mechanisms of caspase activation, *Curr. Opin. Cell. Biol.* 15 (2003) 725–731, <http://dx.doi.org/10.1016/j.ceb.2003.10.009>.